

Crosstalk elimination in the detection of dual-beam optical tweezers by spatial filtering

Dino Ott, S. Nader S. Reihani, and Lene B. Oddershede

Citation: [Review of Scientific Instruments](#) **85**, 053108 (2014); doi: 10.1063/1.4878261

View online: <http://dx.doi.org/10.1063/1.4878261>

View Table of Contents: <http://scitation.aip.org/content/aip/journal/rsi/85/5?ver=pdfcov>

Published by the [AIP Publishing](#)

Articles you may be interested in

[Analysis of optical and electrical crosstalk in small pitch photon trapping HgCdTe pixel arrays](#)

Appl. Phys. Lett. **101**, 261118 (2012); 10.1063/1.4773484

[Auto- and cross-power spectral analysis of dual trap optical tweezer experiments using Bayesian inference](#)

Rev. Sci. Instrum. **83**, 095116 (2012); 10.1063/1.4753917

[Interference and crosstalk in double optical tweezers using a single laser source](#)

Rev. Sci. Instrum. **79**, 083103 (2008); 10.1063/1.2957652

[Single beam optical tweezers setup with backscattered light detection for three-dimensional measurements on DNA and nanopores](#)

Rev. Sci. Instrum. **79**, 063702 (2008); 10.1063/1.2938401

[Twin optical traps for two-particle cross-correlation measurements: Eliminating cross-talk](#)

Rev. Sci. Instrum. **79**, 043103 (2008); 10.1063/1.2898407

GRANVILLE-PHILLIPS®

ADVANCED VACUUM MEASUREMENT SOLUTIONS

Vacuum Gauges:

Convectron®, Micro-Ion®, Stabil-Ion®,
Cold Cathode

Mass Spectrometers:

Vacuum Quality Monitors



www.brooks.com

Introducing the First
Cold Cathode Gauge
worthy of the
Granville-Phillips name!

- Unsurpassed Accuracy
- Predictive & Easy Maintenance



Crosstalk elimination in the detection of dual-beam optical tweezers by spatial filtering

Dino Ott,¹ S. Nader S. Reihani,² and Lene B. Oddershede^{1,a)}

¹Niels Bohr Institute (NBI), University of Copenhagen, Blegdamsvej 17, DK-2100 Copenhagen, Denmark

²Department of Physics, Sharif University of Technology, 11369-9161 Tehran, Iran

(Received 12 March 2014; accepted 6 May 2014; published online 27 May 2014)

In dual-beam optical tweezers, the accuracy of position and force measurements is often compromised by crosstalk between the two detected signals, this crosstalk leading to systematic and significant errors on the measured forces and distances. This is true both for dual-beam optical traps where the splitting of the two traps is done by polarization optics and for dual optical traps constructed by other methods, e.g., holographic tweezers. If the two traps are orthogonally polarized, most often crosstalk is minimized by inserting polarization optics in front of the detector; however, this method is not perfect because of the de-polarization of the trapping beam introduced by the required high numerical aperture optics. Here we present a simple and easy-to-implement method to efficiently eliminate crosstalk. The method is based on spatial filtering by simply inserting a pinhole at the correct position and is highly compatible with standard back focal plane photodiode based detection of position and force. Our spatial filtering method reduces crosstalk up to five times better than polarization filtering alone. The effectiveness is dependent on pinhole size and distance between the traps and is here quantified experimentally and reproduced by theoretical modeling. The method here proposed will improve the accuracy of force-distance measurements, e.g., of single molecules, performed by dual-beam optical traps and hence give much more scientific value for the experimental efforts.

© 2014 AIP Publishing LLC. [<http://dx.doi.org/10.1063/1.4878261>]

I. INTRODUCTION

Dual-beam optical traps have been successfully used to investigate, e.g., the mechanical properties of DNA,^{1,2} DNA protein association,³ and the mechanical action of molecular motors.^{4,5} For these subtle and technically advanced investigations, it is of utmost importance that as much information as possible is retrieved from the data and that data are as accurate as possible, i.e., without systematic errors. Dual optical traps can be constructed in different ways, e.g., by holographic means,⁶ but the most common way is to insert a polarizing beam splitter in the path and hence create two traps with orthogonal polarizations from a single laser source. This is convenient as it is easy, low-cost, and facilitates independent control of the two individual traps.^{7,8} Also, it is an advantage that the two traps come from a single laser source and hence have similar Poynting vector and power fluctuations.

In “single beam” optical traps, it is common and convenient to use the trapping laser beam also for detection of the positions visited by the trapped particle by detecting the forward and un-scattered light by a photodiode placed in the back focal plane. Through proper calibration, one can then deduce the forces acting on the trapped particle.⁹ Force- and distance-detection by photodiodes have significant advantages compared to camera based detection; the detection rates can be significantly higher, thus revealing very fast dynamics, and the acquisition and subsequent data analysis is significantly faster than image-based detection. A similar method is often applied to detect the position of trapped particles in dual

traps with orthogonal polarization. In this case, a polarizing beam splitter, or a polarization filter, is placed in front of the photodiode, thus, in principle, allowing only the signal from one trap to impinge on a particular photodiode. However, a complete separation purely based on polarization optics is not possible: First, polarization optics are not perfect; when using polarizing beam splitters the reflected beam often still contains 1% of the “wrong” polarization. Second and even more problematic, a partial depolarization of the trapping beams occurs due to the high numerical aperture (NA) optics required for obtaining three-dimensional trapping by a single laser beam.¹⁰ This incomplete separation of the signals consequently leads to so-called crosstalk, a parasitic signal originating from the other trap when measuring one specific trap of interest. Depolarization due to high-NA optics, which can reach up to 10% of the integrated focal intensity,¹¹ should be taken seriously as it can represent a severe source of error¹² resulting in a deviation in the measured force magnitude of up to several pN.¹⁰ The parasitic signal changes the voltage signal of a given quadrant or pixel and enters the differential signal used for lateral detection in a non-trivial and systematic manner. As the axial position is normally measured as the total power impinging on the photodiode, the axial positions and forces will be systematically overestimated. These errors are, of course, problematic both while measuring, e.g., physical properties of molecular motors¹³ or weak hydrodynamic interactions between trapped particles.¹⁴

Since crosstalk presents a serious problem to acquisition, several means for signal separation have been presented. These include fast sequential detection of time-multiplexed optical traps,¹⁵ polarization rectification by beam back propagation through the focusing objective,¹⁰ and advanced

^{a)} Author to whom correspondence should be addressed. Electronic mail: oddershede@nbi.dk

signal processing.¹⁶ As a simple, low cost, and efficient alternative to the previously published techniques, we here present a method to perform crosstalk suppression by spatial filtering. The method simply consists of inserting a pinhole in a position that allows only the signal originating from the trap of interest to propagate to the photodiode detector. This new method reduces crosstalk to less than 0.2%, thus performing five times better than standard polarization filtering alone.

II. PRESENTATION OF THE SPATIAL FILTERING METHOD

In typical interferometric detection schemes, the signal is imaged by a lens onto a plane conjugate to the back focal plane (BFP).⁹ This is because space constraints typically do not allow placement of the photodiode directly at the BFP. Therefore, an intermediate plane exists, which is conjugate to the focal plane of the microscope objective, i.e., to the sample plane where the trapping is performed. The trapping beams overlap along most of the optical path. In this intermediate plane, however, the beams are well separated spatially, and filtering is done simply by inserting a pinhole here, as sketched in Figure 1. If the foci of the trapping beams are separated in the sample plane, they will also be separated in this conjugate plane. By accurately positioning the pinhole at the focus of the beam of interest (grey trap in Figure 1, from now on referred to as Trap 1), only this beam will be transmitted to the detection photodiode. The other beam (henceforth denoted Trap 2) will be efficiently obstructed, and crosstalk will be eliminated. The experimental setup is further detailed in Sec. IV.

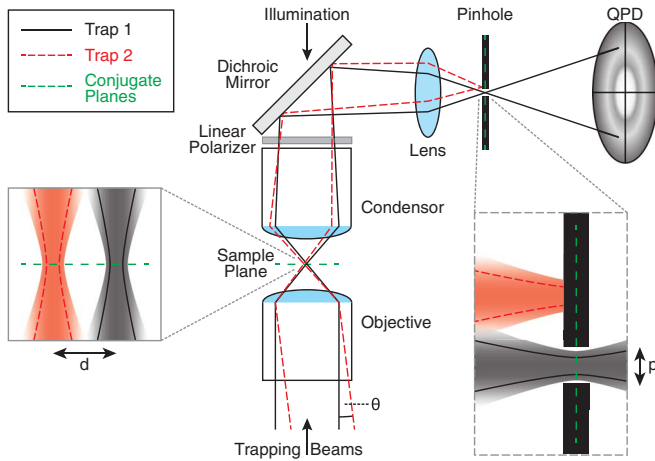


FIG. 1. Illustration of the spatial filtering method. Two independent traps are created in the sample plane by two trapping beams in orthogonal polarization states. Trap 2 enters the objective at an angle θ , which translates to a lateral distance d between the foci. The transmitted light is collected by the microscope condenser. A lens images the back focal plane of the condenser onto a quadrant photodiode for detection of the position of the trapped particle. Blocking the laser beam of Trap 2 by a pinhole with diameter p , located in a plane conjugate to the sample plane, allows for the transmission of Trap 1 to the detector and effectively suppresses crosstalk from Trap 2. Optionally, crosstalk can be further minimized by adding a linear polarizer in front of the QPD.

III. RESULTS

A. Influence of spatial filtering on optical trapping and detection

To ensure that the proposed crosstalk elimination method does not influence the optical trapping and position detection capabilities, a full analysis of the trap characteristics was conducted for a single-beam optical trap with the pinhole installed. For each translational direction, there exists a conversion factor, which allows for conversion from the arbitrary voltage readout from the quadrant photodiode (QPD) to absolute lengths. The exact definition and calculation of the conversion factor is detailed in Sec. IV. It is of great convenience in photodiode-based detection of optically trapped objects if this conversion factor is constant across the interval of data acquisition. To check for this, an experiment was performed where a bead, immobilized on a glass surface, was scanned by a piezo stage through the focus in three dimensions. The relation between the voltage readout from the QPD and the actual position in one of the lateral directions, y , is shown in Figure 2(a). Clearly, there is a large linear range, signifying a constant conversion factor. This was true for all three translational directions. The y -conversion factor should be relatively constant upon small variations in x , and Figure 2(b) confirms that this is indeed the case.

For small particle excursions, an optical trap based on a Gaussian intensity profile exerts an approximately harmonic force, $F = -\kappa x$, on the trapped particle, where κ denotes the trap stiffness and x is the deviation from the equilibrium position. As detailed in Sec. IV, the dynamics of the trapped particle obeys the Langevin equation, and the power spectrum of the time series is well fitted by a Lorentzian function, from which the so-called corner frequency, $f_c = \kappa/2\pi\gamma$, can be found. Here, γ denotes the friction coefficient of the bead in the solution, which can be estimated from Stokes' law if far from any surfaces. To ensure that the spatially filtered Trap 1 retained the "normal" trapping behavior, time series of the positions visited by a bead in Trap 1 were analyzed while Trap 2 was blocked before entering the microscope. The inset of Figure 2(c) shows that the position histogram is well fitted by a Gaussian distribution, hence, the spatially filtered Trap 1 still exerts a harmonic force. Also, experiments with and without the pinhole installed in the optical path were done, to ensure that the insertion of the pinhole leaves the measured corner frequency of Trap 1 unaltered. The result is shown in Figure 2(c), where the two data sets are artificially displaced from each other in the vertical direction. Within the error bars (one standard deviation), f_c , and hence also κ , are unaffected by the presence of the pinhole.

B. Quantification of crosstalk suppression

As a measure of crosstalk, we use the quantity

$$\Psi = \frac{S_{\text{parasitic}}}{S_{\text{total}}}, \quad (1)$$

where the signals $S_{\text{parasitic}}$ and S_{total} denote the parasitic signal and the total signal, respectively. In practice, $S_{\text{parasitic}}$ was measured as the signal that penetrated the pinhole (aligned at Trap

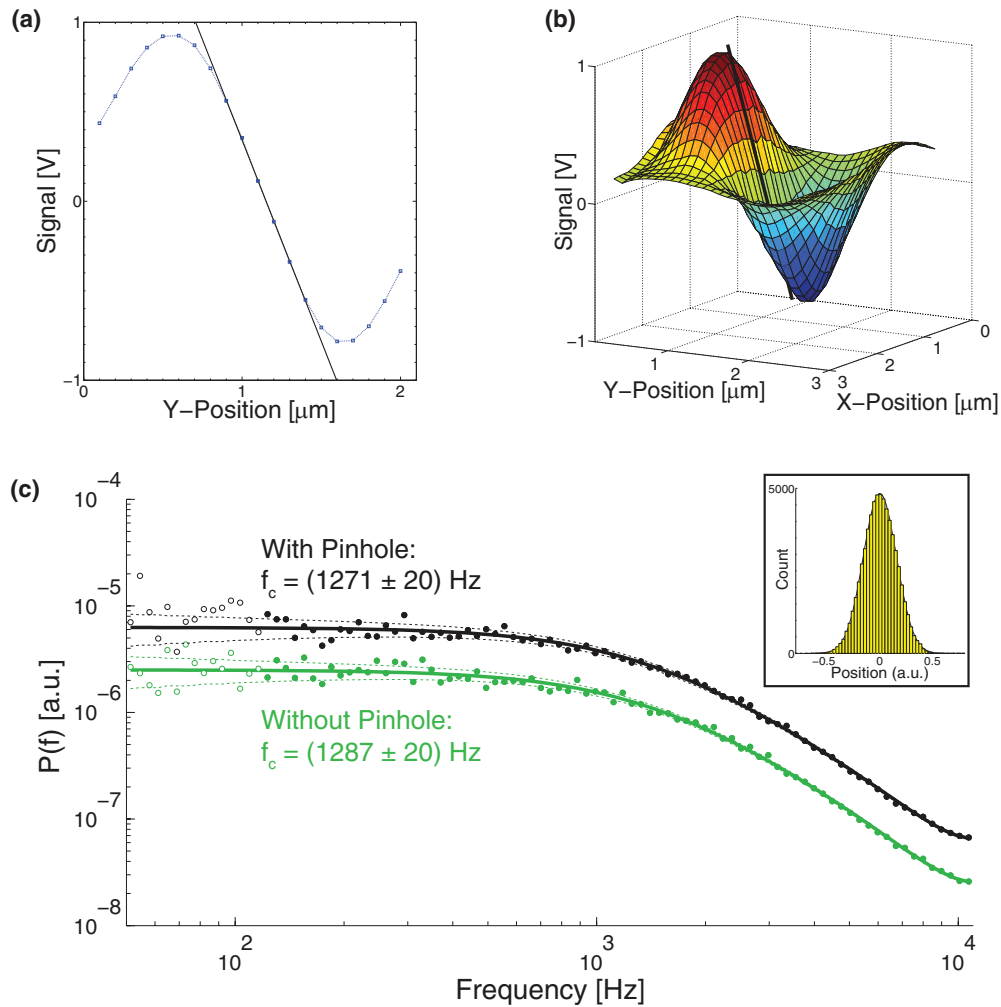


FIG. 2. Influence of pinhole insertion on optical trapping in Trap 1 and photodiode based detection. (a) The raw y-voltage signal from the photodiode as a function of lateral motion of the bead within the trap. The linear region verifies a substantial region with a constant conversion factor. (b) The raw y-signal from the photodiode as a function of movement in both lateral directions. The y-signal shows a linear dependence on the bead's y-displacement from its equilibrium position and only a minor dependency on its displacement along the x-axis. The full line corresponds to graph A. (c) Comparison of power spectra of the time series originating from Trap 1 with and without the pinhole inserted. For visibility, the two plots have been arbitrarily displaced in the vertical direction. The solid line denotes a fit to the data utilizing a Lorentzian function, as detailed in Sec. IV, using the program from Ref. 17. The dotted lines indicate the ± 1 standard deviation expected from theory, filled dots mark data included in the fit, open circles indicate data outside the fitting range. Inset: Histogram of the positions visited by the trapped particle, full line is a Gaussian fit.

1) while Trap 1 was off and Trap 2 was on. Similarly, S_{total} was measured as the signal that penetrated the pinhole while both Trap 1 and Trap 2 were on. In other words, this measure of crosstalk quantifies the contribution of the parasitic signal from Trap 2 to the total measured signal in a dual-trap experiment where both traps are on and where the aim is to measure exclusively the signal originating from Trap 1. The signals were recorded while varying the distance d between the traps. This was done by keeping Trap 1 at a constant position in the center of the field of view (FOV), co-centering the pinhole with Trap 1 for maximum transmission, and subsequently stepwise moving the focus of Trap 2 to the distance d . The signal measured is the total intensity reaching the QPD, $I_{\text{QPD}} = I_1 + I_2 + I_3 + I_4$, which is the sum of the intensities, I_i , $i = \{1, 2, 3, 4\}$, detected by each of the four individual quadrants.

We investigated the influence of the trap separation d on crosstalk for a range of pinhole diameters, $p = 5 \mu\text{m}$,

$10 \mu\text{m}$, $20 \mu\text{m}$, $30 \mu\text{m}$, $50 \mu\text{m}$, $100 \mu\text{m}$, and $150 \mu\text{m}$. The result is plotted in Figure 3(a), which shows crosstalk (Ψ) as a function of distance between the traps, d , for different pinhole diameters. As expected, a maximal crosstalk of 50% is obtained when the beams overlap perfectly ($d = 0$), as both beams pass through the pinhole and Trap 2 contributes with 50% to the total signal. With increasing d the crosstalk, Ψ , decreases (Fig. 3(a)) and goes towards zero for large d . The smaller the pinhole diameter, the more rapid and effective is the crosstalk suppression. To quantify the crosstalk suppression for varying pinhole sizes, we compared the distances Γ , where the crosstalk Ψ had fallen by 3dB, i.e., by 50%, relative to its maximum value at $d = 0$. Figure 3(b) shows Γ as a function of p and indicates a linear relation between Γ and the pinhole diameter for diameters larger than $20 \mu\text{m}$. This linear relation can be used to choose the optimal pinhole size for a certain experimental design. At $p \leq 10 \mu\text{m}$, an oscillatory behavior of $\Psi(d)$ is observed. This probably originates from

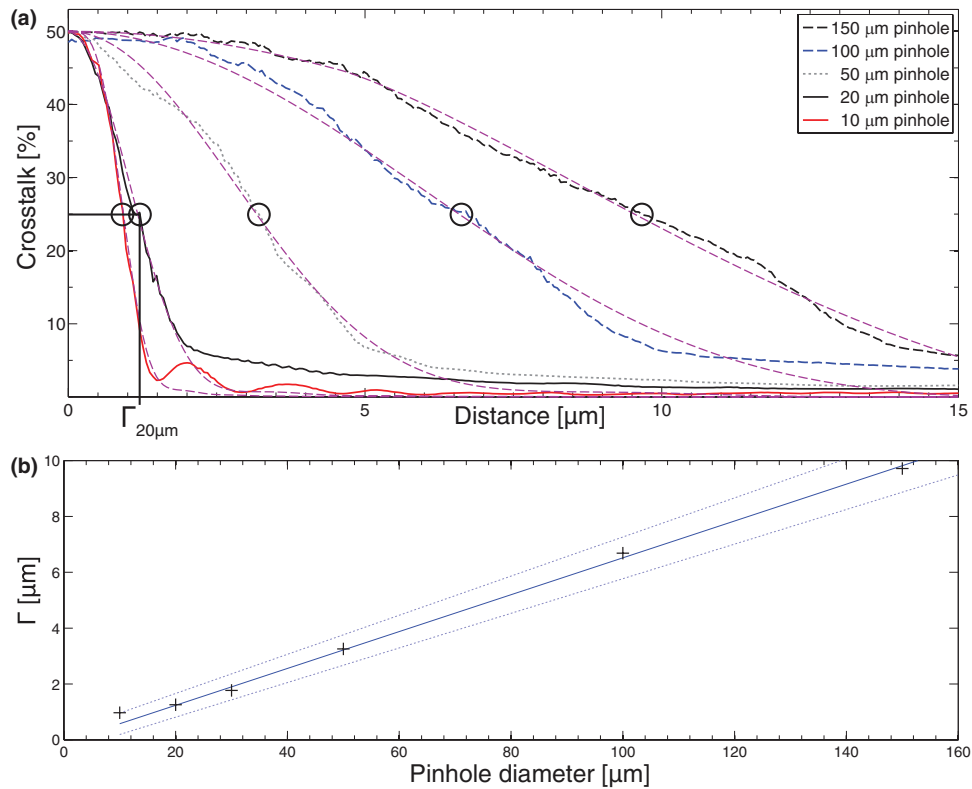


FIG. 3. Crosstalk suppression by spatial filtering. (a) Crosstalk Ψ as a function of distance d for varying pinhole size. All curves are raw data, no smoothing filter was applied. The dashed purple lines are theoretical fits to the experimental data. The 3dB decrease distance, Γ , is shown as a black ring for each pinhole size and explicitly marked for $p = 20 \mu\text{m}$. (b) 3dB decrease distance, Γ , as a function of pinhole diameter, p . The full line shows a linear fit to the data points from $p = 20 \mu\text{m}$ to $150 \mu\text{m}$, the dotted lines denote the 95%-confidence area of the fit. The data point of the $10 \mu\text{m}$ pinhole is located just outside the 95%-confidence area, indicating that for this small pinhole the linear relation does not hold.

diffraction effects and sets a lower limit for the usable pinhole size.

C. Theoretical prediction of crosstalk suppression by spatial filtering

To support the experimental findings, we theoretically modeled the crosstalk suppression by spatial filtering. We modeled the spatial filtering process using a wave optics approach. The optical system was simplified by modeling the lens compounds of both the objective and the condenser as single lenses. The expanded Gaussian-shaped trapping beam entering the objective lens is focused down to a diffraction limited spot. The shape of this focal spot is influenced by the overfilling ratio, i.e., the ratio between the $\frac{1}{e^2}$ -beam diameter and the front aperture of the objective. When the $\frac{1}{e^2}$ -beam diameter matches the aperture diameter, the focal spot is approximately Gaussian-shaped with side lobes of very low intensity. With larger overfilling ratios, the incident intensity profile becomes more uniform and the side lobes in the focal intensity distribution become more pronounced. In other words, the intensity distribution becomes more Airy disk-like, as this is the interference pattern caused by Fraunhofer diffraction of a plane wave with a flat intensity profile at a circular aperture.¹⁸

The focal spot in the sample plane is magnified and imaged into the pinhole plane. This transformation is dictated by

the point spread function of the imaging optics, resulting in an intensity distribution resembling that of an Airy disk, which mathematically can be described as

$$\mathcal{I}(r) = \mathcal{I}_0 \left(\frac{2 J_1(x)}{x} \right)^2, \quad (2)$$

with the peak intensity \mathcal{I}_0 and $J_1(x)$ denoting the Bessel function of the first kind of order one, where x contains both geometrical and optical parameters, i.e., $x = (2\pi/\lambda)ar$, with a being the radius of the circular condenser aperture, λ the wavelength, and r the radial distance from the optical axis measured in the plane of the diffraction pattern.¹⁹

Now, the (d dependent) transmission of the parasitic signal, Ψ_{theory} , can be estimated by computing the 2D-convolution

$$\Psi_{\text{theory}} = \mathcal{I}(r) \star g(r) \quad (3)$$

of the diffraction pattern $\mathcal{I}(r)$ and a two-dimensional circular boxcar function $g(r)$, defined by $g(r < p/2) = 1$ and $g(r > p/2) = 0$, representing the pinhole, which is located in this plane. Two-parameter fits, accounting for the shape of the Airy disk and the pinhole diameter, to the experimentally measured curves are shown in Figure 3(a) (purple dashed lines). The crosstalk, as a function of trap separation distance, is well described by the model; in particular, the initial flat region and the decrease fit quite well. However, the model underestimates the tails of the distribution. This is probably

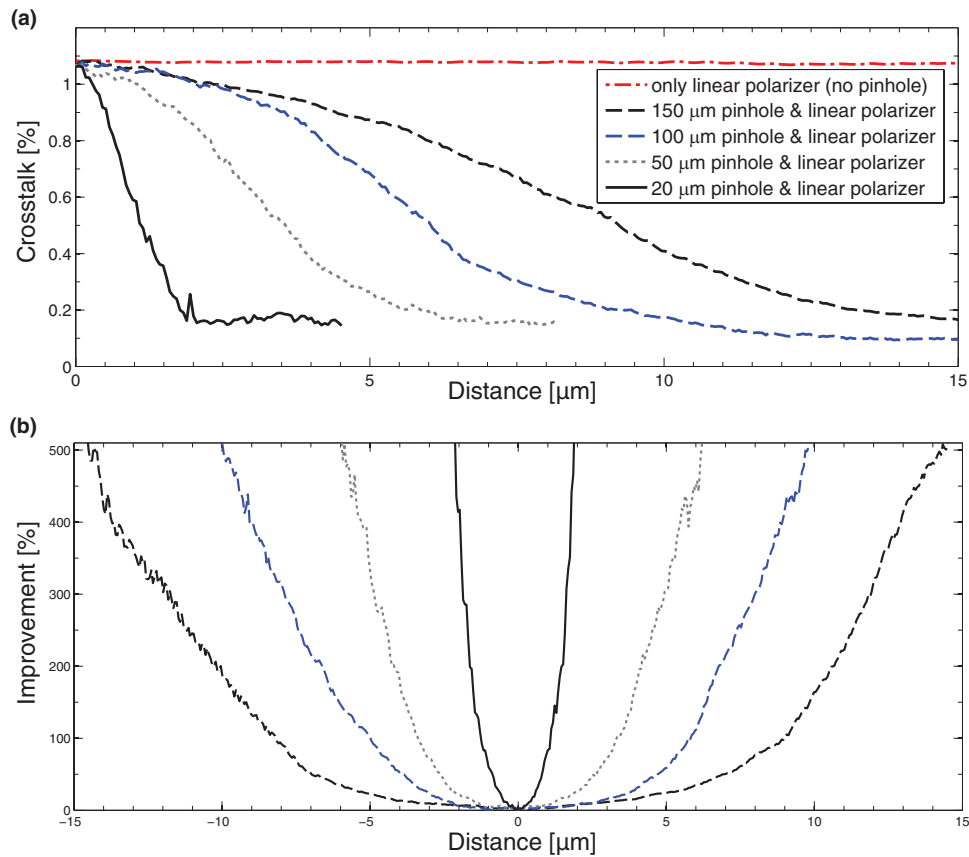


FIG. 4. Combining spatial and polarization filtering for efficient crosstalk suppression. (a) Crosstalk as a function of trap separation distance, d . If only the polarization filtering is performed (dot-dash red line), the crosstalk level is independent of d . Adding also the spatial filtering improves the crosstalk suppression down to a level of 0.2 percent for sufficient trap separation. (b) Crosstalk suppression improvement, Ω , by employing both spatial and polarization filtering compared to employing polarization filtering alone. The improvement was calculated for the data shown in (a) and the legends are the same.

because in the experiments there are inherent aberrations that are not included in the theory and which give rise to more pronounced side lobes.

D. Crosstalk suppression by combining spatial and polarization filtering

The most common way to suppress crosstalk in dual-beam orthogonally polarized optical traps is by inserting polarization optics in front of the photodiode detector and the minimal crosstalk for a well aligned, purely polarization-based filtering is on the order of 1 to 1.5%.¹¹ The efficiency of polarization filtering alone is comparable to that of spatial filtering alone. To obtain an exceptionally high degree of crosstalk suppression, the two methods should be combined, which is straightforward in practice. Here we quantify the crosstalk suppression by such a combination of spatial and polarization filtering. For the experimental measurements of combining spatial and polarization filtering a linear polarizer (extinction ratio $>1 : 10^7$, Thorlabs LPNIR100) was placed in the BFP of the condenser (see Fig. 1).

In accordance with Ref. 11, we obtained a crosstalk level of 1.1% when employing only a linear polarizer and no pinhole for filtering (dot-dashed red line in Figure 4(a)). As expected, this value did not depend on the distance d separating the traps. After inserting the pinhole, the crosstalk de-

creased with increasing trap separation, d , dropping to a value significantly below the level achievable with the polarization optics alone (Fig. 4(a)). Combining spatial filtering with polarization filtering provides crosstalk levels below 0.2% for sufficient trap separation d . Notably, at this very low level of crosstalk, we are limited by electronics noise, not by the pinhole method.

To compare the crosstalk while performing only linear polarization filtering (Ψ_{LP}) to the crosstalk while performing both pinhole based spatial filtering and linear polarization filtering ($\Psi_{PH\&LP}$), we calculated the improvement, Ω :

$$\Omega = \frac{\Psi_{LP} - \Psi_{PH\&LP}}{\Psi_{PH\&LP}}, \quad (4)$$

as a function of trap separation distance d . The result is plotted in Figure 4(b), which shows that the advantage of employing also the spatial filtering increases as the trap separation distance increases. Also, it shows that at trap separations of more than 2 μm , the crosstalk can be reduced by a factor five by spatial filtering with correct pinhole size.

IV. METHODS

A. Optics

The experiments were carried out on a modified inverted microscope (Leica DM IRBE), into which dual-beam

optical tweezers were implemented. The two optical traps, of equal power, were created by splitting a laser beam (1064 nm CW Nd:YVO₄ laser, Spectra Physics J20I-BL-106C-02) into two separate beams, by means of a half-wave-plate followed by a polarizing beam splitter. In the optical path of Trap 2, there was a 1:1-telescope allowing for steering Trap 2: the first lens of the telescope, the “beam steering lens,” was imaged onto the BFP of the objective by the second telescope lens. A LabView-controlled, piezo-actuated linear translation stage (Newport Picomotor, 9066-X-P-M) allowed for precise lateral displacement of this beam steering lens, thus causing a change in the angle of incidence θ into the objective, which then led to a lateral displacement of Trap 2 in the focal plane.⁸ Besides allowing for position control, this layout guaranteed minimal clipping of the beam by the objective entrance aperture when translating the optical trap. The two expanded Gaussian-shaped laser beams with orthogonal polarization states were focused by a high-NA water immersion objective (63X, NA=1.2, Leica HCX PL APO W CORR CS), thus creating the optical trap. An oil immersion condenser (NA = 1.4, Leica S1 551004) collected the transmitted light, whose back focal plane was imaged onto a QPD (Si-PIN photodiode, Hamamatsu S5981).

The sample chamber was made by sandwiching two #1.5 glass cover slips on top of each other using double-sided sticky tape, to form a water-filled perfusion chamber, approximately 80 μm in thickness. All trapping experiments were performed far from any surfaces. The mean diameter of the particles was 0.96 μm (PS03N/9396, Bangs Laboratories).

B. Alignment of pinhole

The pinhole was mounted on actuators with differential drives (Thorlabs ST1XY-D) that allowed for precise three-dimensional translation. An initial coarse positioning of the pinhole, in the plane conjugate to the focal plane, was followed by an iterative positioning process, in which the position was fine-adjusted to maximize the transmitted intensity. The correct alignment of the pinhole with the trap of interest, i.e., Trap 1, could be verified by monitoring the signal while switching Trap 1 on and off or while scanning Trap 2 through the field of view.

C. Calibration

To deduce forces and distances from optical trapping, it is a necessity to perform a calibration. We calibrated the trap through monitoring the thermal fluctuations of the particle within the trap.⁹ The bead fluctuates in the harmonic potential of the optical trap, and its dynamics is well described by the Langevin equation

$$m\ddot{x}(t) + \gamma\dot{x}(t) + \kappa x(t) = F_{\text{therm}}(t), \quad (5)$$

with x being the time-dependent position of the bead, m the bead's mass, γ the friction coefficient given by Stokes' law: $\gamma = 3\pi\eta d$ (d being the diameter of the particle and η the viscosity) if far from any surfaces, and κ the spring constant characterizing the optical trapping potential. $F_{\text{therm}}(t)$ is a ran-

dom and time-dependent force due to stochastic thermal collisions with the solvent. As the trapping is conducted in water, inertia is negligible compared to any of the other terms and the inertial term, $m\ddot{x}(t)$, can safely be neglected.

The position of the bead in the trap was measured by a quadrant photodiode (QPD). The QPD has four photodiodes arranged as quadrants: the difference signals provide the lateral positions of the bead, and the sum of all four signals is proportional to the axial movement of the bead.²³ The raw output from the QPD ($S(t)$) is in volts and needs to be converted into metric units for absolute distance determination ($x(t)$). In a certain range, $S(t)$ and $x(t)$ are linearly proportional and a conversion factor, β , can be determined:

$$x(t) = \beta S(t). \quad (6)$$

The power spectrum of the voltage signal, $S(t)$, obtained in a measurement with finite measurement time T , can be found as

$$P_{\text{exp}}(f) = |\tilde{S}(f)|^2 / T. \quad (7)$$

Here, $\tilde{S}(f)$ denotes the Fourier transform of the signal $S(t)$

$$\tilde{S}(f) = \int_{-T/2}^{T/2} S(t)e^{i2\pi ft} dt. \quad (8)$$

Using Eq. (6), the power spectrum of the experimental data can be written as

$$P_{\text{exp}}(f) = |\tilde{S}(f)|^2 / T = \frac{1}{\beta^2} |\tilde{x}(f)|^2 / T. \quad (9)$$

The theoretical power spectrum of the Langevin equation, $P(f)$, is the expectation value of the experimental power spectrum:

$$P(f) = \langle P_{\text{exp}}(f) \rangle = \frac{A}{f_c^2 + f^2}, \quad (10)$$

where f_c is the so-called corner frequency, $f_c = \kappa/2\pi\gamma$, and $A = \frac{D}{2\pi^2\beta^2}$, with D being the diffusion constant of the bead. D is connected to γ via the Einstein equation

$$D = \frac{k_B T}{\gamma}, \quad (11)$$

where T is the absolute temperature and k_B the Boltzmann constant. A different numerical factor can appear in the equation for A , depending on whether one considers the one-sided or the two-sided power spectral density in the analysis. The above stated formula for A is for the two-sided PSD.

The corner frequency f_c and the conversion factor β can now be determined by fitting the theoretically expected PSD to the experimental data regarding A and f_c as the fitting parameters. In the simplest case of calibrating an optical trap, this would mean a simple Lorentzian fit. However, in practice the photodiode has a pronounced filtering effect²⁴ that needs to be taken into account in the fitting procedure. We used the program from Ref. 17, which takes this filtering effect as well as aliasing and other minor effects into account. Finally, κ can be extracted from f_c (as $f_c = \kappa/2\pi\gamma$) which concludes the calibration.

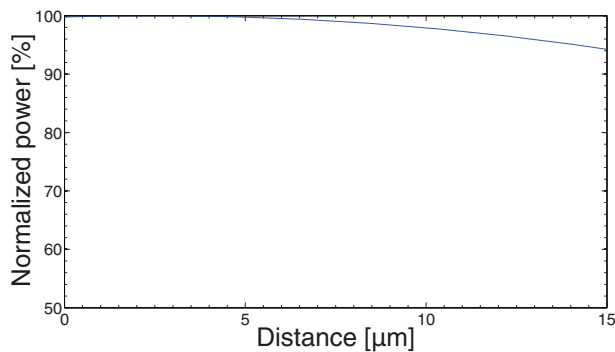


FIG. 5. Calibration curve quantifying the change of power of Trap 2 as a function of distance between Trap 1 and Trap 2. Not taking this power loss into account would lead to an underestimation of the crosstalk.

D. Data analysis

Time series of 3 s of the positions visited by the bead in the trap were recorded at 22 kHz and used for calibration. Based on Allan variance analysis, this is the optimal length and acquisition frequency for the current setup.²⁵ Low frequency mechanical vibrations of the pinhole were omitted by excluding low frequency components below 120 Hz in the fit. Prior to the crosstalk analysis, we subtracted the QPD dark current from the measured integral QPD signal. This was measured prior to each experiment for the chosen analog preamplification of the QPD voltage signal. Also, we compensated for the slight power loss (less than 5%) that occurs when Trap 2 is moved away from the center of the field of view. This power loss is caused by the fact that the BFP of the objective does not coincide with the objective shoulder but is actually located inside the objective (17.50 mm), thus leading to a marginal cutting of the impinging beam when being tilted to move the trap laterally in the focal plane. Disregarding this effect would result in an underestimation of the crosstalk when moving towards to the margins of the field of view. To determine this power loss, we measured the transmitted power as a function of the position of Trap 2. The resulting calibration curve is shown in Figure 5.

V. CONCLUSION

Crosstalk elimination is critical for high precision measurements involving the detection of several laser beams, as it gives rise to the detection of a parasitic signal that adds a systematic error to the readout and hence compromises the accuracy of experiments. This is of specific interest for dual-beam optical traps, where the forces and distances of a trapped object are read off using photodiode detectors. We present a method based on spatial filtering for efficient elimination of crosstalk. The method simply consists of inserting a pinhole in a plane conjugate to the focal plane. This spatial filtering does not alter the forces and distances measured from a single trap, and the linear range between displacement and readout from the photodiode detector is preserved. Both direct experimental measurements and theoretical modeling confirmed that the spatial filtering effec-

tively minimizes crosstalk; the larger the trap-trap distance, the larger the suppression. We provide tools for selecting the proper pinhole size for a certain acceptable crosstalk level. If the two traps have orthogonal linear polarization, spatial filtering alone is approximately as efficient polarization filtering, which is commonly used. However, if the two methods are combined, which in practice is very easy, then the crosstalk is extremely efficiently suppressed; in fact, the combined method gives a factor five improvement compared to the standard linear polarization filtering alone. The spatial filtering technique can readily be adapted to other implementations of optical traps than just dual-beam optical traps. In principle, the method can easily be extended to detect the signal from any spatially separated arrangement of multiple optical traps, for instance holographic optical tweezers (HOTs).^{6,20} Normally, the detection of forces and displacement of objects in multiple optical traps is done by means of a camera, because it has been difficult to separate the signals from the multiple laser beams using photodiodes. With this spatial filtering, it should be possible to separate the signal from each trap and detect it individually with a photodiode, which has distinct advantages over camera detection, e.g., higher temporal and spatial resolution^{21,22} as well as easier data analysis. Hence, we believe the presented signal filtering scheme will prove quite useful for future more accurate optical tweezers experiments.

ACKNOWLEDGMENTS

The authors acknowledge financial support from the University of Copenhagen Excellence Program and technical support by Erik Grønbaek Jacobsen and Axel Boisen.

- ¹P. Gross, N. Laurens, L. B. Oddershede, U. Bockelmann, E. J. G. Peterman, and G. J. L. Wuite, *Nat. Phys.* **7**, 731 (2011).
- ²I. Heller, G. Sitters, O. D. Broekmans, G. Farge, C. Menges, W. Wende, S. W. Hell, E. J. G. Peterman, and G. J. L. Wuite, *Nat. Methods* **10**, 910 (2013).
- ³J. Sung, S. Sivaramakrishnan, A. R. Dunn, and J. A. Spudich, *Methods in Enzymology*, 1st ed. (Elsevier Inc., 2010), Vol. 475, pp. 321–75.
- ⁴J. T. Finer, R. M. Simmons, and J. A. Spudich, *Nature (London)* **368**, 113 (1994).
- ⁵J. Zhou, V. Schweikhard, and S. M. Block, *Biochim. Biophys. Acta* **1829**, 29 (2013).
- ⁶J. E. Curtis, B. A. Koss, and D. G. Grier, *Opt. Commun.* **207**, 169 (2002).
- ⁷K. Visscher, S. P. Gross, and S. M. Block, *IEEE J. Sel. Top. Quantum Electron.* **2**, 1066 (1996).
- ⁸K. C. Neuman and S. M. Block, *Rev. Sci. Instrum.* **75**, 2787 (2004).
- ⁹F. Gittes and C. F. Schmidt, *Opt. Lett.* **23**, 7 (1998).
- ¹⁰P. Mangeol and U. Bockelmann, *Rev. Sci. Instrum.* **79**, 083103 (2008).
- ¹¹M. Atakhorrami, K. M. Addas, and C. F. Schmidt, *Rev. Sci. Instrum.* **79**, 043103 (2008).
- ¹²K. Bahlmann and S. W. Hell, *Appl. Phys. Lett.* **77**, 612 (2000).
- ¹³J. R. Moffitt, Y. R. Chemla, D. Izhaky, and C. Bustamante, *Proc. Natl. Acad. Sci. U.S.A.* **103**, 9006 (2006).
- ¹⁴J.-C. Meiners and S. R. Quake, *Phys. Rev. Lett.* **82**, 2211 (1999).
- ¹⁵D. Ruh, B. Tränkle, and A. Rohrbach, *Opt. Express* **19**, 21627 (2011).
- ¹⁶Y. von Hansen, A. Mehlich, B. Pelz, M. Rief, and R. R. Netz, *Rev. Sci. Instrum.* **83**, 095116 (2012).
- ¹⁷P. M. Hansen, I. M. Tolić-Nørrelykke, H. Flyvbjerg, and K. Berg-Sørensen, *Comput. Phys. Commun.* **174**, 518 (2006).

- ¹⁸V. N. Mahajan, *J. Opt. Soc. Am. A* **3**, 470 (1986).
- ¹⁹M. Born and E. Wolf, *Principles of Optics: Electromagnetic Theory of Propagation, Interference and Diffraction of Light* (Cambridge University Press, Cambridge, 1999).
- ²⁰K. Dholakia and T. Čižmár, *Nat. Photon.* **5**, 335 (2011).
- ²¹S. Keen, J. Leach, G. Gibson, and M. J. Padgett, *J. Opt. A: Pure Appl. Opt.* **9**, S264 (2007).
- ²²C. Pacoret and S. Régnier, *Rev. Sci. Instrum.* **84**, 081301 (2013).
- ²³A. Pralle, M. Prummer, E.-L. Florin, E. H. K. Stelzer, and J. K. H. Hörber, *Microsc. Res. Tech.* **44**, 378 (1999).
- ²⁴K. Berg-Sørensen, L. Oddershede, E.-L. Florin, and H. Flyvbjerg, *J. Appl. Phys.* **93**, 3167 (2003).
- ²⁵F. Czerwinski, A. C. Richardson, and L. B. Oddershede, *Opt. Express* **17**, 13255 (2009).